Atmos. Chem. Phys. Discuss., https://doi.org/10.5194/acp-2019-250
Manuscript under review for journal Atmos. Chem. Phys.
Discussion started: 25 March 2019

A new parameterization scheme of the real part of the ambient aerosols refractive index

Gang Zhao[1], Tianyi Tan[2], Weilun Zhao[1], Song Guo[2], Ping Tian[3], Chunsheng Zhao[1*]

1 Department of Atmospheric and Oceanic Sciences, School of Physics, Peking University, Beijing, China

2 State Key Joint Laboratory of Environmental Simulation and Pollution Control, College of Environmental Sciences and Engineering, Peking University, Beijing 100871, China

3 Beijing Key Laboratory of Cloud, Precipitation and Atmospheric Water Resources, Beijing 100089, China

[*]Correspondence to: Chunsheng Zhao (zcs@pku.edu.cn)

Abstract

The refractive index of ambient aerosols, which directly determines the aerosol optical properties, is widely used in atmospheric models and remote sensing. Traditionally, the real part of the refractive index (RRI) is mainly parameterized by the measurement of ambient aerosol main inorganic components. In this paper, the characteristics of the ambient aerosol RRI are studied based on the field measurement in the East China. Results show that the ambient aerosol RRI varies significantly between 1.36 and 1.56. The direct aerosol radiative forcing is estimated to vary by 40% corresponding to the variation of the measured aerosol RRI. We find that the ambient aerosol RRI is highly related with the aerosol effective density (ρ_{eff}) rather than the main chemical components. However, parameterization schemes of the ambient aerosol RRI by ρ_{eff} are not available due to the lack of corresponding simultaneous field measurements. For the first time, the size-resolved ambient aerosol RRI and ρ_{eff}

are measured simultaneously by our designed measurement system. A new parameterization scheme of the ambient aerosols RRI using ρ_{eff} is proposed. The measured and parameterized RRI agree well with the correlation coefficient of 0.76. Knowledge of the ambient aerosol RRI would improve our understanding of the ambient aerosol radiative effects.

1 Introduction

Atmospheric aerosols can significantly influence the reginal air quality and climate system by scattering and absorbing the solar radiation (Seinfeld et al., 1998). However, estimation of the aerosol radiative effects remains large uncertainties due to the high temporal and spatial variations in aerosol microphysical properties (Levoni et al., 1997). The complex refractive index (RI), which directly determines the aerosol scattering and absorbing abilities (Bohren and Huffman, 2007), is one of the most important microphysical parameters of aerosol optics and radiation. RI is widely employed in atmospheric models and remote sensing (Zhao et al., 2017). When estimating the direct aerosol radiative forcing (DARF), many studies show that great uncertainties may arise due to small uncertainties in the real prat of the RI (RRI). For non-absorbing particles, it was found that a small perturbation in RRI (0.003) can lead to an uncertainty of 1% in DARF (Zarzana et al., 2014). An increment of 12% in the DARF occurred when the RRI increases from 1.4 to 1.5 (Moise et al., 2015). Therefore, it is necessary to measure or parameterize the ambient aerosol RRI with high accuracy.

Traditionally, the RRI is determined by aerosol chemical components (Han et al., 2009). Inversely, information of RRI may be helpful for the knowledge of ambient aerosol chemical information. Up until now, there is limit information about the size-resolved RRI ($\widetilde{\mathrm{RRI}}$) of ambient particles. However, many studies find that ambient aerosols of different size have different properties such as shape (Peng et al., 2016), chemical composition (Hu et al., 2012) and density (Qiao et al., 2018). Characteristics of the ambient aerosol $\widetilde{\mathrm{RRI}}$ were not well studied yet.

The RRI of mono-component particle is defined by (Liu and Daum, 2008):

$$\frac{n^2-1}{n^2+2}=\frac{N_A\alpha}{3M}\rho_{eff} \qquad (1),$$

Atmos. Chem. Phys. Discuss., https://doi.org/10.5194/acp-2019-250
Manuscript under review for journal Atmos. Chem. Phys.
Discussion started: 25 March 2019

where N_A is the universal Avagadro's number, α is the mean molecular polarizability, M is the molecular weight of the material and ρ_{eff} is the mass effective density of the chemical component. For the ambient aerosol with multiple components, a common approach to calculate the aerosol effective RRI by linear volume average (Hand and Kreidenweis, 2002;Liu and Daum, 2008;Hanel, 1968;Wex et al., 2002), which calculates the RRI by integrating partial refractive index n_i weighted with the volume fraction f_i:

$$n_e = \sum_i f_i n_i \qquad (2).$$

The ρ_{eff} is one of the crucial parameters in aerosol thermo-dynamical and optical models. The ρ_{eff} can also be used to infer the ambient particle aging process (Peng et al., 2016). Based on equation 1, the aerosol ρ_{eff} is directly related to the aerosol RRI. Few studies measure the ambient aerosol RRI and ρ_{eff} simultaneously. So far, parameterizations of the RRI by ρ_{eff} using the simultaneous measurements are not available. Real-time measurements of the size-resolved ρ_{eff} ($\widetilde{\rho_{eff}}$) combined with the $\widetilde{RRI}$ can help to better understand the relationship between the aerosol RRI and ρ_{eff}.

In this study, the aerosol $\widetilde{RRI}$ and $\widetilde{\rho_{eff}}$ are measured simultaneously during a field measrument conducted in Taizhou in the East China. The ambient aerosol $\widetilde{RRI}$ is measured by our designed system, which combines a differential mobility analyzer (DMA) and a single particle soot photometer (SP2) (Zhao et al., 2018b). The $\widetilde{\rho_{eff}}$ is measured by using a centrifugal particle mass analyzer (CMPA) and a scanning mobility particle sizer (SMPS). The characteristic of the $\widetilde{RRI}$ and $\widetilde{\rho_{eff}}$ are analyzed in this study. For the first time, a parameterization scheme of the RRI by the ρ_{eff} using the simultaneous measurement is proposed. Based on the measured variability of the measured RRI, we estimated the corresponding variation of the aerosol direct aerosol radiative forcing, which to some extent give valuable knowledge for the aerosol radiative effects.

The structure of this study is as follows: the descriptions of the instrument setup is given in section 2.1-2.3. The methodology of evaluating the aerosol optical properties and radiative effects corresponding to the variations of the measured RRI is shown in section 2.4 and 2.5 respectively. Section 3.1 describes the characteristics of the measured the $\widetilde{RRI}$ and $\widetilde{\rho_{eff}}$. Section 3.3 propose the parameterization of the aerosol RRI. The corresponding variations in aerosol optical properties and radiative effects corresponding to the variations of the measured RRI are both discussed in section 3.4.

Atmos. Chem. Phys. Discuss., https://doi.org/10.5194/acp-2019-250
Manuscript under review for journal Atmos. Chem. Phys.
Discussion started: 25 March 2019

2 Data and Methods

2.1 Description of the measurement campaign

The measurement was conducted in a suburban site Taizhou (119°57'E, 32°35'N), as shown in fig. S1(a), which lies in the south end of the Jianghuai Plain in the central Eastern China. It is located on the north east of the megacity Nanjing with a distance of 118 km. Another megacity Shanghai is 200 km away from Taizhou in the southeastern direction. The industrial area between Nanjing and Shanghai has experienced severe pollutions in the past twenty years. The average Moderate Resolution Imaging Spectroradiometer (MODIS) aerosol optical depth data at 550nm over the year 2017, as shown in fig. S1(b), also reflects that the measurement site is more polluted than the surrounding areas.

During the field campaign, all of the instruments were placed in a container, in which the temperature was well controlled within 24±2 °C. The sample air was collected from a PM_{10} impactor (Mesa Labs, Model SSI2.5) mounted on the top of the container and then passed through a Nafion dryer tube to ensure that the relative humidity of the sample particles was controlled below 30%.

Along with the measurement of the $\widetilde{\mathrm{RRI}}$ and $\widetilde{\rho_{\mathrm{eff}}}$, the aerosol scattering coefficients (σ_{sca}) at three different wavelengths (450, 525 and 635 nm) were measured by an nephelometer (Aurora 3000, Ecotech, Australia) (Müller et al., 2011) at a resolution of 5 minutes. The scattering truncation and non-Lambertian error was corrected using the method in Ma et al. (2011). The mass concentration of the black carbon (m_{BC}) is measured by an aethalometer (AE33) (Drinovec et al., 2015) and the σ_{abs} is recorded every minute. The aerosol water-soluble ions (NH_4^+, SO_4^{2-}, NO_3^-, Cl^-) of $PM_{2.5}$ were measured by an In situ Gas and Aerosol Compositions Monitor (TH-GAC3000, China). The mass concentration of elementary carbon and organic carbon (OC) were measured using a thermal optical transmittance aerosol carbon analyzer (ECOC, Focused Photonics Inc.). The concentrations of Organic matters (OM) are achieved through multiplying OC concentration by 1.4 (Hu et al., 2012). The time resolution of the aerosol composition measurement was one hour.

An automatic weather station was located next to the aerosol measurement container. The wind speed, wind direction, temperature (T) and relative humidity (RH) were measured in 1-minute time resolution.

Atmos. Chem. Phys. Discuss., https://doi.org/10.5194/acp-2019-250
Manuscript under review for journal Atmos. Chem. Phys.
Discussion started: 25 March 2019

2.2 Measuring the $\widetilde{\mathrm{RRI}}$

A coupling DMA-SP2 system was employed to measure the aerosol $\widetilde{\mathrm{RRI}}$ from 24th, May to 18th, June in 2018. This system is introduced elsewhere by Zhao et al. (2018b) and a brief description is presented here. As schematically shown in fig. S2, the monodispersed aerosols selected by a DMA (Model 3081, TSI, USA) are drawn into a SP2 to measure the corresponding scattering properties. The SP2 is capable of distinguishing the pure scattering aerosols from the black carbon (BC) containing aerosols by measuring the incandescence signals. For the pure scattering aerosol, the scattering strength (S) measured by SP2 is expressed as:

$$S = C \cdot I_0 \cdot (\sigma_{45^o} + \sigma_{135^o}) \qquad (3),$$

where C is a constant that is determined by the instrument response character; I_0 is the instrument's laser intensity; σ_{45^o} and σ_{135^o} is the scattering function of the sampled aerosol at 45° and 135°, respectively;. From Mie scattering theory , aerosol size and RRI directly determine the scattering function at a given direction. Inversely, the aerosol RRI can be retrieved when the aerosol size and scattering strength are determined. This system can measure the ambient aerosol $\widetilde{\mathrm{RRI}}$ with uncertainty less than 0.02 (Zhao et al., 2018b).

Before the measurement, this system is calibrated with ammonia sulfate (RRI=1.52). The relationships between the diameter and the measured scattering peak height are shown in fig. S3.

2.3 Measuring the $\widetilde{\rho_{eff}}$

The $\widetilde{\rho_{eff}}$ is measured by a Centrifugal Particle Mass Analyzer (CPMA, version 1.53, Cambustion Ltd, UK) in tandem with a Scanning Mobility Particle Sizer (SMPS) system from 12th, June to 18th, June in 2018. The ρ_{eff} is defined as

$$\rho_{eff} = \frac{m_p}{\frac{\pi}{6} \times d_m^3} \qquad (4),$$

Where m_p is the particle mass and d_m is the aerosol mobility diameter selected by DMA.

The controlling of the CPMA-SMPS system is achieved by self-established Labview software. The CPMA is set to scan twelve different aerosol mass at 1.0, 1.4, 2.0, 2.9, 4.2, 5.9, 8.5, 12.1, 17.2, 24.6, 35.0 and 50.0 fg every five minutes respectively. The SMPS scan the aerosol diameters between 60nm and 500nm every 5 minute, which results in a period of one hour for measuring the effective density of different mass.

Atmos. Chem. Phys. Discuss., https://doi.org/10.5194/acp-2019-250
Manuscript under review for journal Atmos. Chem. Phys.
Discussion started: 25 March 2019

At the beginning of the field measurement, the CPMA-SMPS system is calibrated using the PSL particles with different mass. The corresponding measured effective densities of PSL particles are 1.04 and 1.07 g/cm^3, which agree well with the PSL material density of 1.05 g/cm^3.

2.4 Calculate aerosol optical properties using different RRI

The aerosol optical properties are highly related to the RRI. From Mie scattering theory, the variation in aerosol RRI may result in significant variations in the aerosol optical properties, such as aerosol extinction coefficient (σ_{ext}), the σ_{sca}, the single scattering albedo (SSA), and the asymmetry factor (g) (Bohren and Huffman, 2007). SSA is defined as the ratio of σ_{sca} to σ_{ext}, which reflects concentration of the absorbing aerosol (Tao et al., 2014) to some extent. The g expresses the distribution of the scattering light intensity in different directions (Zhao et al., 2018a).

In this study, the sensitivity studies of the aeorsol optical proprties to the aerosol RRI are carried out by employing the Mie scattering theory. The input variables of Mie scattering model includes the aerosol PNSD and BC mixing state and aerosol complex refractive index. The Mie model can calculate the σ_{ext}, σ_{sca}, SSA and g. The mixing state of the ambient BC comes from the measurements of the DMA-SP2 system. All of the aerosols are divided into pure scattering aerosols and BC-containing aerosols. The BC-containing aerosols are assumed to be core-shell mixed. As for the RI of BC, 1.8+0.54i is used (Kuang et al., 2015). With this, the aerosol σ_{ext}, σ_{sca}, SSA and g at different RRI values can be calculated.

2.5 Estimating the aerosol DARF

In this study, the DARF under different aerosol RRI conditions is estimated by the Santa Barbara DISORT (discrete ordinates radiative transfer) Atmospheric Radiative Transfer (SBDART) model (Ricchiazzi et al., 1998). Under the cloud-free conditions, DARF at the TOA is defined as the difference between radiative flux under aerosol-free conditions and aerosol present conditions:

$$\mathrm{DARF} = (\mathrm{f_a}\downarrow - \mathrm{f_a}\uparrow) - (\mathrm{f_n}\downarrow - \mathrm{f_n}\uparrow) \quad (5),$$

where $f_a\downarrow$ and $f_a\uparrow$ are the downward and upward radiative irradiance with aerosol respectively; $f_n\downarrow$ and $f_n\uparrow$ correspond to the radiative irradiance values under aerosol free conditions (Kuang et al., 2016).

Atmos. Chem. Phys. Discuss., https://doi.org/10.5194/acp-2019-250
Manuscript under review for journal Atmos. Chem. Phys.
Discussion started: 25 March 2019

Input data for the model are shown below. The vertical profiles of temperature, pressure and water vapor, which are the mean results of the radiosonde observations at Taizhou site during the field measurement. Vertical distributions of aerosol σ_{ext}, SSA and g with a resolution of 50 m, are resulted from the calculation using the Mie Model and parameterized aerosol vertical distributions. More details of calculating the optical profiles can refer to Zhao et al. (2018a). The surface albedo adopt the mean results of MODIS V005 Climate Modeling Grid (CMG) Albedo Product (MCD43C3) at the area of Taizhou from May, 2017 to April, 2018. The other default values are used in the simulation (Ricchiazzi et al., 1998).

3 Results and Discussions

3.1 The Measurements Results

The overview of the measurement is shown in fig. S4. During the measurement, the mean wind speed is relatively low with 2.13±1.13 m/s. The prevailing speed is south wind and south east wind. The average T and RH are 23±6.4ºC and 74.0±18.7% respectively. The T and RH show evident diurnal cycles as illustrated in fig. S5 (a) and (b). The T gets its peak values at 15:00 in the afternoon and the lowest value at 4:00 at night. The RH exhibited opposite trend. During the campaign, the rain occurred at the night of 25th, 28th, 31st in May, which can be reflected by the high RH shown in fig. S4 (b). The mean m_{BC} is 3.82±3.37 μg/m^3 and the mean σ_{sca} at 525 nm is 276±230 Mm^{-1}. Both the m_{BC} and σ_{sca} shows evident diurnal variation based on fig. S5 (c) and (d), which is highly related to the development of the mixing layer height, the local emission and the ambient aging process. The m_{BC} and σ_{sca} peak at around 7:00 in the morning and reach the valley at 15:00 in the afternoon. The peak values of the m_{BC} and σ_{sca} are about three time of the minimum value correspondingly.

Based on the m_{BC} and σ_{sca} time series, there were total two pollution episodes occurred during this campaign. The first episode happens from 28th, May to 30th, May and the maximum values of m_{BC} and σ_{sca} reach 20 μg/m^3 and 1197 Mm^{-1}, which is about 5 times the concentrations of the mean aerosol loading. The second period of pollution happens from the night of 4th, June to 7th June, and doesn't last long. The corresponding m_{BC} and σ_{sca} reaches 14 μg/m^3 and 1210Mm^{-1}. A moderate polluted condition between 1st, June and 3rd, June is observed. Another moderate pollution happens during the 11th, June and 14th, when the $\widetilde{RRI}$ and $\widetilde{\rho_{eff}}$ are measured simultaneously.

Fig. 1 shows the time series of the concurrently measured $\widetilde{\mathrm{RRI}}$ and $\widetilde{\rho_{\mathrm{eff}}}$. During this period, the σ_{sca} is relatively low with a mean value of 167±74 Mm^{-1}. The $\widetilde{\mathrm{RRI}}$ and $\widetilde{\rho_{\mathrm{eff}}}$ vary from 1.34 to 1.54 and the $\widetilde{\rho_{\mathrm{eff}}}$ ranges between 1.21 to 1.80 g/cm^3. From fig. 1, the measured RRI shows the same variation pattern with the ρ_{eff}. Both the $\widetilde{\mathrm{RRI}}$ and $\widetilde{\rho_{\mathrm{eff}}}$ increase with the diameter, which may indicate that the aerosol chemical composition varies among different aerosol particle size.

As for the $\widetilde{\mathrm{RRI}}$, the measured RRI values of ambient aerosol for 200nm, 300nm and 450nm show large variations from 1.36 to 1.56. The corresponding mean RRI values for 200nm, 300nm and 450nm are 1.425±0.031, 1.435±0.041, 1.47±0.059 as shown in fig. S4 (e). When comparing the probability distribution of the RRI for different diameter in fig. 3 (b), (d) and (f), we find that the RRI is more dispersed when the particle size increases, implicating that the aerosol compositions become complicated when the aerosol get aged. Fig. 3 (a), (c) and (e) give diurnal variation of the $\widetilde{\mathrm{RRI}}$ values at different particle sizes of 200 nm, 300 nm and 450 nm. The RRI shows slightly diurnal cycles for different diameters. They reach the peak at about 15:00 in the morning and fall to the valley at around 9:00 in the afternoon.

The range of the measured RRI (1.34~1.56) is a little larger than the literature values. The past measurement of the ambient aerosol RRI values varies between 1.4 and 1.6 (Dubovik, 2002;Guyon et al., 2003;Zhang et al., 2016) over different measurement site. This is the first time that such high variations in ambient aerosol RRI were observed at one site.

The $\widetilde{\rho_{\mathrm{eff}}}$ shows almost the same diurnal variations as the $\widetilde{\mathrm{RRI}}$ as shown fig. S6. The diurnal variations of the $\widetilde{\rho_{\mathrm{eff}}}$ is more dispersed because the time period of measuring the $\widetilde{\rho_{\mathrm{eff}}}$ is shorter (7 days) comparing with the time of $\widetilde{\mathrm{RRI}}$ (28 days). It is evident that the ρ_{eff} increased with particle size.

3.2 Aerosol Chemical Composition versus the RRI

From equation (1) and (2), the aerosol RRI can be determined by aerosol chemical composition (Liu and Daum, 2008). Many studies calculate the RRI using the measurement results of the relative contributions of aerosol chemical composition (Yue et al., 1994;Hanel, 1968;Guyon et al., 2003;Stelson, 1990;Wex et al., 2002). However, there is no comparison between the RRI calculated

Atmos. Chem. Phys. Discuss., https://doi.org/10.5194/acp-2019-250
Manuscript under review for journal Atmos. Chem. Phys.
Discussion started: 25 March 2019

from chemical composition and real-time measurement until now. In this study, the relationship between the measured RRI and the mass fraction of each ion components is investigated.

As illustrated in fig. 3, the RRI tend to increase with the OM mass fraction ratio, which implies that the OM may play an important role in aerosol scattering properties. This is in agreement with the Aldhaif et al. (2018), where the aerosol OM contributes a lot to the ambient aerosol mass concentrations. The RRI have implicit relationship with the mass fraction of the σ_{sca} at 525 nm, SO_4^{2-}, Cl^-, and NO_3^-. The mass ratio of NH_4^+ seems to be negatively correlated with the RRI. At the same time, the measured RRI values have no clear relationship with the absolute mass concentrations of the main aerosol chemical components, as shown in fig. S7.

The RRI is also calculated by applying the method proposed by Stelson (1990), in which the bulk chemical composition is used. The comparison between the calculated RRI and the measured RRI is shown in fig. S8. It can be noticed that the calculated RRI and the measured RRI doesn't agree well. There are several reasons that may cause the discrepancies. The first reason might be that the aerosol chemical information used in the method is the average mass of whole aerosol population. The aerosol chemical composition may vary significantly among different size. Secondly, the OM of the ambient aerosols is very complicated and the influence of the OM on the aerosol RRI has not been studied well. Therefore, more research is necessary when parameterizing the ambient aerosol RRI with the measured aerosol chemical composition.

3.3 Parameterizing the RRI using ρ_{eff}

As shown in fig. 1, there is good consistence between the variation of the measured $\widetilde{\mathrm{RRI}}$ and $\widetilde{\rho_{eff}}$. When defining the specific refractive index Re with $\mathrm{Re} = \frac{n^2-1}{n^2+2}$, we found that the Re is highly correlated with ρ_{eff} by a R^2 equaling 0.76 (fig. 4). The linear relationships between the Re and ρ_{eff} is:

$$\mathrm{Re} = \frac{n^2-1}{n^2+2} = 0.18\rho \qquad (5).$$

Based on equation (5) and fig. 4 the aerosol RRI can be parameterized by the ρ_{eff} with high accuracy and the uncertainties of the calculated RRI using equation 5 can be constrained within 0.025.

The aerosol ρ_{eff} is easier to be measured, and equation 5 might be used as a good probe of parameterizing the RRI.

In the previous, Liu and Daum (2008) summarized some of the measured RRI and the ρ_{eff}, and parameterized the RRI as

$$\frac{n^2-1}{n^2+2} = 0.23\rho^{0.39} \qquad (6).$$

The feasibility of this scheme is tested here and the results are shown in fig. S9. The measured and parameterized RRI using the method of Liu and Daum (2008) deviated from 1:1 line. The deviations might be caused by that the proposed parameterization scheme by Liu and Daum (2008) does not base on the simultaneous field measurement.

3.4 Influence of RRI Variation on Aerosol Optical Properties and Radiative Properties

The measured RRI varies between 1.34 and 1.56 during the field campaign. The corresponding aerosol optical properties are estimated. Fig. 5 gives the variation of the aerosol σ_{sca}, SSA and g. From fig. 5, the σ_{sca} varies from 162 Mm^{-1} to 308 Mm^{-1}. The SSA varies between 0.843 and 0.895, which matches the variations of the dry aerosol SSA for different aerosol size distributions in the North China Plain (NCP) (Tao et al., 2014). As for the aerosol g, it decreases from 0.667 to 0.602 with the increment of the aerosol RRI. The ambient g values in the NCP are found within 0.55 and 0.66 (Zhao et al., 2018a). Thus, the variations of the RRI have significant influence on the g. The aerosol optical properties change significantly with the variation of the ambient aerosol RRI.

The DARF values under different RRI are also estimated and the results are illustrated in fig. 5(b). When the aerosol RRI increases from 1.4 to 1.5, the DARF varies from -6.17 to -8.35, corresponding to 15% variation in DARF. This values are in accordance with the work of Moise et al. (2015), who estimate that an increment of 12% in the DARF occurs when the RRI varies from 1.4 to 1.5. The DARF can change from -4.9 w/m^2 to -10.14 w/m^2 when the aerosol RRI increase from 1.34 to 1.56, which corresponding to 40% variation in DARF. We recommend that the real-time measured RRI be used rather than a constant RRI when estimating the ambient aerosol optical and radiative properties.

4 Conclusions

The ambient aerosol RRI is a key parameter in determining the aerosol optical properties and knowledge of it can help constrain the uncertainties in aerosol radiative forcing. In this study, the

Atmos. Chem. Phys. Discuss., https://doi.org/10.5194/acp-2019-250
Manuscript under review for journal Atmos. Chem. Phys.
Discussion started: 25 March 2019

ambient aerosol $\widetilde{\mathrm{RRI}}$ were measured at Taizhou, in the Jianghuai Plain of China by using a DMA in tandem with a SP2 from 24th, May to 18th, June in 2018.

Results show that the ambient aerosol RRI varies over a wide range between 1.34 and 1.56. The RRI increases slowly with the increment of the aerosol diameter. The mean aerosol RRI values are 1.425±0.031, 1.435±0.041, 1.47±0.059 at 200nm, 300nm and 450nm respectively. Probability distributions of the RRI show that the RRI is more dispersed with the increment of aerosol dimeter, which reflect the complexing aging processing of the ambient aerosol. The aerosol optical properties change significantly and the DARF is estimated to vary by 40% corresponding to the variation of the measured ambient aerosol RRI. The real-time measured RRI should be used rather than a constant RRI when estimating the ambient aerosol optical and radiative properties.

Traditionally, the ambient aerosol RRI is mainly calculated by using the corresponding measured main chemical inorganic compositions of aerosols. We find that the ambient aerosol RRI is highly related with the ρ_{eff} rather than the main chemical compositions of aerosols. There is discrepancy between the measured and parameterized RRI using the traditional method. This might be resulted from two reasons. The first one is that the aerosol chemical information used for calculation is the total aerosol loading. The aerosol chemical compositions may change significantly among different size. Another one is that the influence of OM of ambient aerosols is not considered. The RRI of OM varies significantly for different compositions (Moise et al., 2015).

Despite that the RRI is related with the ρ_{eff}, parameterization scheme of the ambient aerosol RRI using ρ_{eff} is not available due to the lack of simultaneously measurement. For the first time, the $\widetilde{\mathrm{RRI}}$ and $\widetilde{\rho_{\mathrm{eff}}}$ were measured simultaneously using our designed system. The $\widetilde{\rho_{eff}}$ is measured during the field campaign by employing a CMPA and a SMPS from 12th, June to 18th, June in 2018.

A new parameterization scheme of the ambient aerosol RRI using the ρ_{eff} is proposed based on the field measurement results. The measured and parameterized RRI agree well with the correlation coefficient of 0.76. This simple scheme is reliable and ready to be used in the calculation of aerosol optical and radiative properties. The corresponding measurement results can also be further used in climate model.

Atmos. Chem. Phys. Discuss., https://doi.org/10.5194/acp-2019-250
Manuscript under review for journal Atmos. Chem. Phys.
Discussion started: 25 March 2019

Atmospheric Chemistry and Physics Discussions

Competing interests. The authors declare that they have no conflict of interest.

Data availability. The data used in this study is available when requesting the authors.

Author contributions. GZ, CZ, WZ and SG designed and conducted the experiments; PT, TY and GZ discussed the results.

Acknowledgments. This work is supported by the National Natural Science Foundation of China (41590872) and National Key R&D Program of China (2016YFC020000:Task 5).

References

Aldhaif, A. M., Stahl, C., Braun, R. A., Moghaddam, M. A., Shingler, T., Crosbie, E., Sawamura, P., Dadashazar, H., Ziemba, L., Jimenez, J. L., Campuzano-Jost, P., and Sorooshian, A.: Characterization of the Real Part of Dry Aerosol Refractive Index Over North America From the Surface to 12 km, Journal of Geophysical Research: Atmospheres, 10.1029/2018jd028504, 2018.

Bohren, C. F., and Huffman, D. R.: Absorption and Scattering by a Sphere, in: Absorption and Scattering of Light by Small Particles, Wiley-VCH Verlag GmbH, 82-129, 2007.

Drinovec, L., Močnik, G., Zotter, P., Prévôt, A. S. H., Ruckstuhl, C., Coz, E., Rupakheti, M., Sciare, J., Müller, T., Wiedensohler, A., and Hansen, A. D. A.: The "dual-spot" Aethalometer: an improved measurement of aerosol black carbon with real-time loading compensation, Atmospheric Measurement Techniques, 8, 1965-1979, 10.5194/amt-8-1965-2015, 2015.

Dubovik, O.: Variability of absorption and optical properties of key aerosol types observed in worldwide locations, J.atmos.sci, 59, 590-608, 2002.

Guyon, P., Boucher, O., Graham, B., Beck, J., Mayol-Bracero, O. L., Roberts, G. C., Maenhaut, W., Artaxo, P., and Andreae, M. O.: Refractive index of aerosol particles over the Amazon tropical forest during LBA-EUSTACH 1999, Journal of Aerosol Science, 34, 883-907, 10.1016/s0021-8502(03)00052-1, 2003.

Atmos. Chem. Phys. Discuss., https://doi.org/10.5194/acp-2019-250
Manuscript under review for journal Atmos. Chem. Phys.
Discussion started: 25 March 2019

Han, Y., Lü, D., Rao, R., and Wang, Y.: Determination of the complex refractive indices of aerosol from aerodynamic particle size spectrometer and integrating nephelometer measurements, Applied Optics, 48, 4108-4117, 10.1364/AO.48.004108, 2009.

Hand, J. L., and Kreidenweis, S. M.: A New Method for Retrieving Particle Refractive Index and Effective Density from Aerosol Size Distribution Data, Aerosol Sci. Technol., 36, 1012-1026, 10.1080/02786820290092276, 2002.

Hanel, G.: REAL PART OF MEAN COMPLEX REFRACTIVE INDEX AND MEAN DENSITY OF SAMPLES OF ATMOSPHERIC AEROSOL PARTICLES, Tellus, 20, 371-&, 10.3402/tellusa.v20i3.10016, 1968.

Hu, M., Peng, J., Sun, K., Yue, D., Guo, S., Wiedensohler, A., and Wu, Z.: Estimation of size-resolved ambient particle density based on the measurement of aerosol number, mass, and chemical size distributions in the winter in Beijing, Environ Sci Technol, 46, 9941-9947, 10.1021/es204073t, 2012.

Kuang, Y., Zhao, C. S., Tao, J. C., and Ma, N.: Diurnal variations of aerosol optical properties in the North China Plain and their influences on the estimates of direct aerosol radiative effect, Atmos. Chem. Phys., 15, 5761-5772, 10.5194/acp-15-5761-2015, 2015.

Kuang, Y., Zhao, C. S., Tao, J. C., Bian, Y. X., and Ma, N.: Impact of aerosol hygroscopic growth on the direct aerosol radiative effect in summer on North China Plain, Atmospheric Environment, 147, 224-233, 2016.

Levoni, C., Cervino, M., Guzzi, R., and Torricella, F.: Atmospheric aerosol optical properties: a database of radiative characteristics for different components and classes, Appl Opt, 36, 8031-8041, 1997.

Liu, Y., and Daum, P. H.: Relationship of refractive index to mass density and self-consistency of mixing rules for multicomponent mixtures like ambient aerosols, Journal of Aerosol Science, 39, 974-986, 10.1016/j.jaerosci.2008.06.006, 2008.

Ma, N., Zhao, C. S., Nowak, A., Müller, T., Pfeifer, S., Cheng, Y. F., Deng, Z. Z., Liu, P. F., Xu, W. Y., Ran, L., Yan, P., Göbel, T., Hallbauer, E., Mildenberger, K., Henning, S., Yu, J., Chen, L. L., Zhou, X. J., Stratmann, F., and Wiedensohler, A.: Aerosol optical properties in the North China Plain during

Atmos. Chem. Phys. Discuss., https://doi.org/10.5194/acp-2019-250
Manuscript under review for journal Atmos. Chem. Phys.
Discussion started: 25 March 2019

HaChi campaign: an in-situ optical closure study, Atmos. Chem. Phys., 11, 5959-5973, 10.5194/acp-11-5959-2011, 2011.

Moise, T., Flores, J. M., and Rudich, Y.: Optical properties of secondary organic aerosols and their changes by chemical processes, Chemical Reviews, 115, 4400-4439, 2015.

Müller, T., Laborde, M., Kassell, G., and Wiedensohler, A.: Design and performance of a three-wavelength LED-based total scatter and backscatter integrating nephelometer, Atmos. Meas. Tech., 4, 1291-1303, 10.5194/amt-4-1291-2011, 2011.

Peng, J., Hu, M., Guo, S., Du, Z., Zheng, J., Shang, D., Levy Zamora, M., Zeng, L., Shao, M., Wu, Y.-S., Zheng, J., Wang, Y., Glen, C. R., Collins, D. R., Molina, M. J., and Zhang, R.: Markedly enhanced absorption and direct radiative forcing of black carbon under polluted urban environments, Proceedings of the National Academy of Sciences, 113, 4266-4271, 10.1073/pnas.1602310113, 2016.

Qiao, K., Wu, Z., Pei, X., Liu, Q., Shang, D., Zheng, J., Du, Z., Zhu, W., Wu, Y., Lou, S., Guo, S., Chan, C. K., Pathak, R. K., Hallquist, M., and Hu, M.: Size-resolved effective density of submicron particles during summertime in the rural atmosphere of Beijing, China, Journal of Environmental Sciences, 10.1016/j.jes.2018.01.012, 2018.

Ricchiazzi, P., Yang, S., Gautier, C., and Sowle, D.: SBDART: A Research and Teaching Software Tool for Plane-Parallel Radiative Transfer in the Earth's Atmosphere, Bulletin of the American Meteorological Society, 79, 2101-2114, 10.1175/1520-0477(1998)079<2101:sarats>2.0.co;2, 1998.

Seinfeld, J. H., Pandis, S. N., and Noone, K.: Atmospheric Chemistry and Physics: From Air Pollution to Climate Change, Environment Science & Policy for Sustainable Development, 40, 26-26, 1998.

Stelson, A. W.: Urban aerosol refractive index prediction by partial molar refraction approach, Environ.sci.technol, 24:11, 1676-1679, 1990.

Tao, J. C., Zhao, C. S., Ma, N., and Liu, P. F.: The impact of aerosol hygroscopic growth on the single-scattering albedo and its application on the NO2 photolysis rate coefficient, Atmos. Chem. Phys., 14, 12055-12067, 10.5194/acp-14-12055-2014, 2014.

Wex, H., Neusüß, C., Wendisch, M., Stratmann, F., Koziar, C., Keil, A., Wiedensohler, A., and Ebert, M.: Particle scattering, backscattering, and absorption coefficients: An in situ closure and sensitivity

Atmos. Chem. Phys. Discuss., https://doi.org/10.5194/acp-2019-250
Manuscript under review for journal Atmos. Chem. Phys.
Discussion started: 25 March 2019

study, Journal of Geophysical Research: Atmospheres, 107, LAC 4-1-LAC 4-18, 10.1029/2000jd000234, 2002.

Yue, G. K., Poole, L. R., Wang, P. H., and Chiou, E. W.: STRATOSPHERIC AEROSOL ACIDITY, DENSITY, AND REFRACTIVE-INDEX DEDUCED FROM SAGE-II AND NMC TEMPERATURE DATA, J Geophys Res-Atmos, 99, 3727-3738, 10.1029/93jd02989, 1994.

Zarzana, K. J., Cappa, C. D., and Tolbert, M. A.: Sensitivity of Aerosol Refractive Index Retrievals Using Optical Spectroscopy, Aerosol Sci. Technol., 48, 1133-1144, 10.1080/02786826.2014.963498, 2014.

Zhang, G., Bi, X., Qiu, N., Han, B., Lin, Q., Peng, L., Chen, D., Wang, X., Peng, P., apos, an, Sheng, G., and Zhou, Z.: The real part of the refractive indices and effective densities for chemically segregated ambient aerosols in Guangzhou measured by a single-particle aerosol mass spectrometer, Atmospheric Chemistry and Physics, 16, 2631-2640, 10.5194/acp-16-2631-2016, 2016.

Zhao, G., Zhao, C., Kuang, Y., Tao, J., Tan, W., Bian, Y., Li, J., and Li, C.: Impact of aerosol hygroscopic growth on retrieving aerosol extinction coefficient profiles from elastic-backscatter lidar signals, Atmospheric Chemistry and Physics, 17, 12133-12143, 10.5194/acp-17-12133-2017, 2017.

Zhao, G., Zhao, C., Kuang, Y., Bian, Y., Tao, J., Shen, C., and Yu, Y.: Calculating the aerosol asymmetry factor based on measurements from the humidified nephelometer system, Atmospheric Chemistry and Physics, 18, 9049-9060, 10.5194/acp-18-9049-2018, 2018a.

Zhao, G., Zhao, C., Zhao, W., and Hello, W.: Method to measure the size-resolved real part of aerosol refractive index, Atmos. Meas. Tech. Discuss., 2018, 1-20, 10.5194/amt-2018-399, 2018b.

Atmos. Chem. Phys. Discuss., https://doi.org/10.5194/acp-2019-250
Manuscript under review for journal Atmos. Chem. Phys.
Discussion started: 25 March 2019

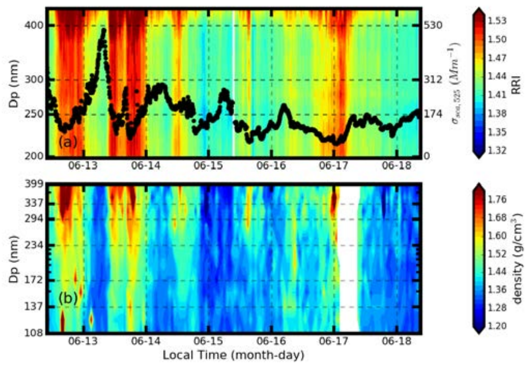

Figure 1. Time series of the measured (a) size-resolved RRI in filled color, σ_{sca} at 525nm in black dotted line and (b) the size-resolved ρ_{eff}.

Atmos. Chem. Phys. Discuss., https://doi.org/10.5194/acp-2019-250
Manuscript under review for journal Atmos. Chem. Phys.
Discussion started: 25 March 2019

Atmospheric Chemistry and Physics
Open Access
Discussions

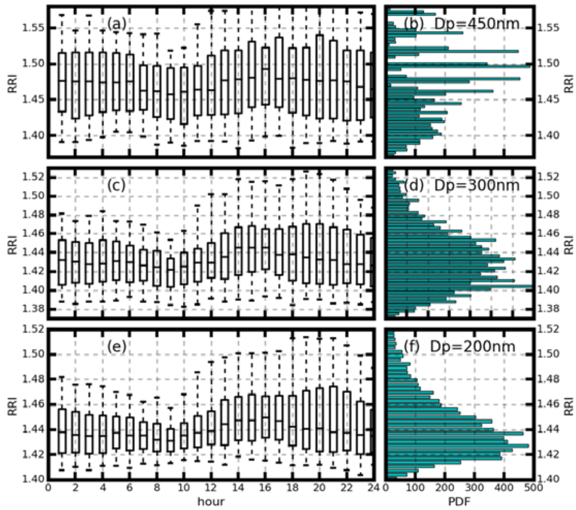

Figure 2. Daily variations of the RRI (a), (c) (e), and the probability distribution of the measured RRI (b), (d) (f) for the (a), (b) 200 nm, (c), (d) 300 nm, and (e), (f) 450nm aerosol respectively. The box and whisker plots represent the 5th, 25th, 75th and 95th percentiles.

Atmos. Chem. Phys. Discuss., https://doi.org/10.5194/acp-2019-250
Manuscript under review for journal Atmos. Chem. Phys.
Discussion started: 25 March 2019

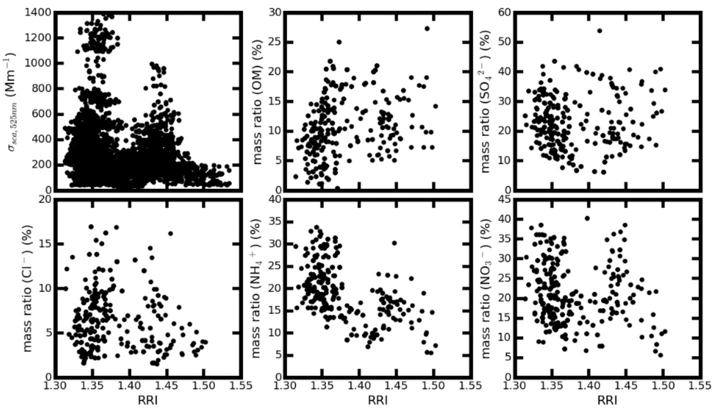

Figure 3. Comparison the measured RRI at 300nm with the measured (a) σ_{sca} at 525nm, mass fraction of (b) OM, (c) SO_4^{2-}, (d) Cl^-, (e) NH_4^+ and (f) NO_3^-.

Atmos. Chem. Phys. Discuss., https://doi.org/10.5194/acp-2019-250
Manuscript under review for journal Atmos. Chem. Phys.
Discussion started: 25 March 2019

Atmospheric Chemistry and Physics
Open Access
Discussions

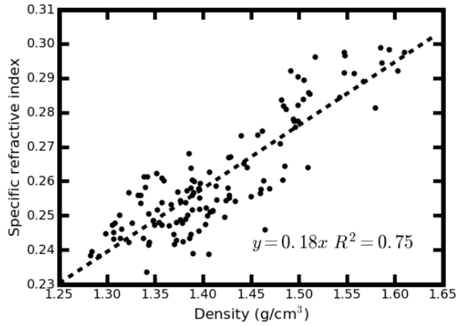

406

407 **Figure 4.** Comparison between the measured density and specific refractive index Re.

408

Atmos. Chem. Phys. Discuss., https://doi.org/10.5194/acp-2019-250
Manuscript under review for journal Atmos. Chem. Phys.
Discussion started: 25 March 2019

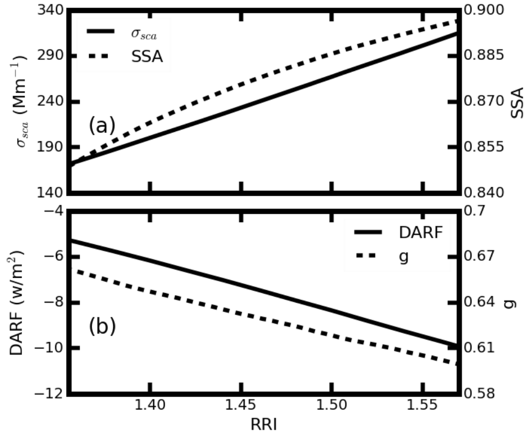

Figure 5. Variations of the estimated (a) σ_{sca} in solid line, SSA in dotted line, (b) g in dotted line, and DARF in solid line for different aerosol RRI.